



Research Paper

Performance of finned tubes used in low-pressure capillary-assisted evaporator of adsorption cooling system



Poovanna Cheppudira Thimmaiah, Amir Sharafian, Wendell Huttema, Chantal Osterman, Ameer Ismail, Aashkaran Dhillon, Majid Bahrami*

Laboratory for Alternative Energy Conversion (LAEC), School of Mechatronic Systems Engineering, Simon Fraser University, BC V3T 0A3, Canada

HIGHLIGHTS

- Performance of capillary-assisted evaporator in adsorption cooling systems is investigated.
- External heat transfer coefficient has positive correlation to chilled water inlet temperature.
- Internal heat transfer coefficient is the bottleneck of the capillary-assisted evaporator.
- Up to 89% of the overall thermal resistance is due to the internal heat transfer resistance.
- Tubes with higher fin density and height provide the lowest overall heat transfer resistance.

ARTICLE INFO

Article history:

Received 22 January 2016

Revised 25 May 2016

Accepted 6 June 2016

Available online 7 June 2016

Keywords:

Capillary-assisted tube

Thermal resistances

Low-operating pressure evaporator

Adsorption cooling system

ABSTRACT

Adsorption cooling systems (ACS) are a viable alternative to vapor compression refrigeration cycles (VCRCs) where low-grade waste heat is readily available. In an ACS, which works with water as a refrigerant, the operating pressure is quite low (~ 1 kPa). Under such low evaporation pressures, the height of a water column affects the water saturation pressure and, consequently, its saturation temperature, which can severely affect the performance of an ACS. This makes the design of evaporators of ACS different from those of conventional VCRCs. One practical solution in low pressure (LP) evaporators is to use capillary-assisted tubes. In this study, three enhanced tubes with different fin geometries (fin spacing and fin height), and a plain tube as a benchmark, are tested for different chilled water inlet temperatures. The results show that enhanced tubes have 9.8–21 times lower external convective heat transfer resistances compared to the plain tube. In addition, the enhanced tube with the highest fin height (Turbo Chil-26 FPI) has 33% lower external convective resistance than that with lower fin height (GEWA-KS-40 FPI). The major finding of this study is that up to 89% of the overall thermal resistance in the enhanced tubes is due to the internal convective resistance. This clearly indicates that the main bottleneck in the performance of a LP evaporator is the convective heat resistance inside the tube. Therefore, the internal heat transfer coefficient and internal surface area of enhance tubes should be increased to enhance the performance of the LP evaporator and overall specific cooling power (SCP) of ACS.

© 2016 Elsevier Ltd. All rights reserved.

1. Introduction

A vapor compression refrigeration cycle (VCRC) is the dominant heating, ventilation and air-conditioning (HVAC) technology accounting for around 38% of energy consumption in the U.S building sector [1]. Vapor-compression equipment account for 99% of space-cooling energy consumption [2]. In transportation sector, a

VCRC in a vehicle air conditioning (A/C) system can add up to 5–6 kW peak power draw [3] on an internal combustion engine (ICE). Also, in an ICE of a light-duty vehicle about 40% of the fuel energy is wasted in the form of exhaust gas and about 30% of the fuel energy is dissipated through the engine coolant [4]. To reduce vehicle fuel consumption and utilize some of this waste heat, a thermally-driven ACS can replace a conventional VCRC. A portion of the waste heat of an ICE is sufficient to run the ACS and generates the cooling power (around 1 TR [5]) required for the vehicle A/C applications. The substitute for the compressor of a VCRC is adsorber bed(s) in which a refrigerant (adsorbate), such as water or methanol, is adsorbed at the surface of an adsorbent,

* Corresponding author at: School of Mechatronic Systems Engineering, Simon Fraser University, # 4300, 250-13450 102nd Avenue, Surrey, BC V3T0A3, Canada.

E-mail addresses: pthimmai@sfu.ca (P. Cheppudira Thimmaiah), asharafi@sfu.ca (A. Sharafian), mbahrami@sfu.ca (M. Bahrami).

Nomenclature

A	heat transfer surface area (m^2)	T_{wall}	average wall temperature
A/C	air conditioning	T_{ref}	average liquid refrigerant temperature
ACS	adsorption cooling system	t	time (s)
c_p	heat capacity at constant pressure (J/kg K)	U	overall heat transfer coefficient ($\text{W/m}^2 \text{K}$)
C	capacity rate (W/K)	VCRC	vapor compression refrigeration cycle
ΔT_{LM}	log mean temperature difference (K)	W	gap between the two fins (m)
FPI	fins per inch	h_o	external heat transfer coefficient ($\text{W/m}^2 \text{K}$)
ICE	internal combustion engine	h_i	internal heat transfer coefficient ($\text{W/m}^2 \text{K}$)
\dot{m}	mass flow rate (kg/s)	ε	effectiveness (%)
NTU	number of transfer units		
P	pressure (Pa)	<i>Subscripts</i>	
\dot{Q}	total heat transfer rate (W)	chilled	chilled water
\dot{q}	heat transfer rate (W)	evap	evaporator
r	radius (m)	i	in
H	height of the fin (m)	o	out
k	thermal conductivity of the tube material (W/m K)	min	minimum
L	length of the tube (m)		
T	temperature ($^{\circ}\text{C}$)		

such as zeolite, silica gel, or activated carbon. Most of these materials are non-toxic, non-corrosive, and inexpensive [6], which makes ACS a safe and environmentally friendly technology. Among the existing refrigerants, water has the highest enthalpy of evaporation (latent heat). However, the saturation pressure of water at temperatures below 100°C , where the evaporator of an A/C system operates, is below atmospheric pressure. Typically an ACS evaporator operates between 3 and 20°C , and has the operating pressure ranging from 0.76 to 2.34 kPa, respectively [7]. Under such operating conditions, a conventional evaporator seizes to perform efficiently and can severely reduce the performance of an ACS [8,9]. Accordingly, an ACS that uses water as the refrigerant requires a low-operating pressure (LP) evaporator. LP evaporator is an integral component of an ACS for achieving higher specific cooling power (SCP) [10]. A LP evaporator can be a flooded type, where liquid water (refrigerant) covers the evaporator tubes and boiling occurs due to natural convection [11,12] for a typical wall superheat temperature of 5 K.

Accumulation of liquid water in a flooded-type LP evaporator creates a water column, which results in a hydrostatic pressure difference between the liquid water-vapor interface and the bottom of the water column. This hydrostatic pressure changes the saturation temperature and pressure of the water. As a result, the cooling power generation of an ACS drastically reduces. To have a uniform water saturation temperature, the static pressure of the water in the LP evaporator should be minimized. Two practical solutions to resolve this issue are: (i) falling film evaporation, and (ii) capillary-assisted evaporation. Florides et al. [13] developed a falling film evaporator operating at 0.9 kPa for an absorption machine in which the refrigerant was showered on vertical tubes. Castro et al. [14] also used falling film evaporator technology at an operating pressure of 1.0 kPa for an absorption machine but the refrigerant was sprayed on horizontal tubes. Falling film evaporators succeed in avoiding the influence of the liquid column on the evaporation and provide high heat transfer coefficient [15–18] specifically for large cooling capacities in a low footprint. However, uniform distribution of refrigerant on horizontal tubes, parasitic power consumption (by internal pumps and circulators), and liquid spray equipment make the falling film evaporators impractical for an ACS installed in a light-duty vehicle A/C system.

Low-operating pressure capillary-assisted evaporation for ACS applications is a relatively novel concept and there are only a few studies available in the literature. Sabir et al. [19–21] studied

the capillary-assisted evaporation on the inner surface of the tube for a vapor absorption chiller and achieved a maximum cooling power of 0.7 kW. The evaporator used air as the heat transfer fluid and due to high pressure drop, the refrigerant had to overcome the flow resistance before reaching the absorber. Capillary-assisted flow and evaporation inside circumferential rectangular micro-grooves were studied by Xia et al. [22,23]. They immersed a finned tube with outside circumferential micro-grooves into a pool of liquid to investigate the effects of immersion depth, evaporation pressure, and superheating degree on the performance of the evaporator. Their experimental results showed that the evaporation heat transfer coefficient has a positive correlation with the evaporation pressure, and a negative correlation with the superheating and immersion depth. Wang et al. [24] developed an evaporator for a silica gel-water ACS based on the work shown in Refs. [22,23]. They claimed that the evaporation heat transfer coefficient was about 5000 $\text{W}/(\text{m}^2 \text{K})$. Lanzerath et al. [25,26] studied a combination of finned tubes and thermal coating for capillary-assisted evaporation at low pressures. Their investigation showed a strong dependency of the total heat transfer coefficient on the water filling level. Their study also established that the combination of macroscopic fin structures and micro porous coatings yielded an evaporation heat transfer coefficient of 5500 $\text{W}/(\text{m}^2 \text{K})$, which is 11 times higher than that of a plain tube with the same outer diameter [6]. Sabir and Bwalya [20] observed that internally powder coated evaporator resulted in much better performance and overall heat transfer coefficient when compared to internally open groove evaporators with deep and shallow grooves. Schnabel et al. [7] evaluated different evaporator concepts for adsorption systems, and capillary-assisted evaporation was one among them. They achieved a maximum cooling power of 1.2 kW while maintaining the operating pressure between 1.1 and 1.7 kPa. The tubes in their study involved both outer and inner structures but Schnabel et al. did not clearly distinguish the effect of inner and outer heat transfer.

The aforementioned studies focused only on enhancing the heat transfer from the external surface of the tubes and they did not report the importance of the effects of thermal resistances to the heat transfer. Therefore, this study attempts to fill this gap in the literature. To generate cooling, the heat has to be transferred from the chilled liquid water flowing inside the tube to the tube wall, and finally, to the refrigerant. The main goals of this research are to evaluate the thermal resistances to the heat flow, such as

external heat transfer resistance, $1/(h_o A_o)$, and the overall heat transfer resistance, $1/(UA)$, in LP evaporators. Enhancements due to continuous parallel fins on the external surface of the tube increase the tube wall conductive resistance. Finally, the internal heat transfer resistance, $1/(h_i A_i)$, should be determined. The importance of the thermal resistances has never been assessed before for LP capillary-assisted evaporation in ACS applications.

In this study, three enhanced tubes with different fin height and fin spacing, and a plain tube, as benchmark, are tested under different operating conditions. In addition, a parametric study is conducted on the selected tube under different chilled water inlet temperatures. The dependence of the external heat transfer coefficient (h_o) under varying liquid water level is presented in this paper. The estimation of thermal resistances of three tested commercially available tubes (Turbo Chil- 26 FPI, Turbo Chil-40 FPI and GEWA-KS-40 FPI) in the application of LP capillary-assisted evaporators are one of the novel contributions of this research.

2. Capillary-assisted evaporation

Due to surface tension inside a rectangular-groove, the liquid-vapor interface forms a curved surface, which leads to a pressure jump across the interface. This pressure jump can be calculated by the augmented Young-Laplace equation [27]. The curvature increases gradually along the circumferential direction of the groove, creating a pressure gradient due to meniscus deformation [27], which is responsible for the upward flow of the liquid. As schematically shown in Fig. 1, the extended meniscus region can be divided into three sub-regions (I) the non-evaporating region, (II) the evaporating thin film region, and (III) the bulk region. The most heat is transferred in region II, where the liquid film is extremely thin and the thermal resistance is extremely low. As the heat flux imposed on the thin film region increases, the evaporation and heat transfer rates through the evaporating thin film also increase [28]. More information on the mechanisms of heat transfer in capillary assisted grooved tubes can be found elsewhere [22,27,29–31].

3. Experimental details

A schematic of capillary-assisted evaporation is shown in Fig. 2, where an enhanced tube with external fins and small fin spacing is in contact with a pool of liquid. Due to capillary action, the liquid covers the outside surface of the tube. Chilled liquid water provided by a temperature control system (TCS) is circulated inside the tube and heat is transferred to the thin liquid film on the outside of the tube, leading to evaporation.

A capillary-assisted LP evaporator built in the Laboratory for Alternative Energy Conversion (LAEC) is shown in Fig. 3. The evaporator tube consisted of a four-pass arrangement with a total length of 1.54 m. Capillary evaporation takes place at the free surface of the tube helping to maintain the evaporation heat transfer

rate as the water level decrease. The tube was placed horizontally at the bottom of the box to minimize the water height as shown in Fig. 3b. Type T thermocouples (Omega, model #5SRTC-TT-T-36-36) with accuracy of 0.75% of the reading in °C, and a pressure transducer with 0.13–3330 kPa operating range (MKS Baratron® Capacitance Manometer, Type 722B) and accuracy of 0.5% of the reading were used to record the temperature and pressure variations at the locations shown in Fig. 3. A positive displacement flow meter (FLO-MEC, Model #OM015S001-222) with the accuracy of 0.5% of reading was employed to measure the mass flow rate of the chilled water. The thermocouples used to measure the outside wall temperature of the tubes were placed at 90° apart at two different cross sections as shown in Figs. 2 and 3.

A schematic diagram of the experimental setup is shown in Fig. 4. The experimental test bed was designed to measure the external heat transfer coefficient (h_o) and the overall heat transfer coefficient (U) of the evaporator. The setup consisted of a TCS and a variable speed pump to provide a constant temperature chilled water to the evaporator at different mass flow rates. A control valve was used to regulate the pressure inside the evaporator. A

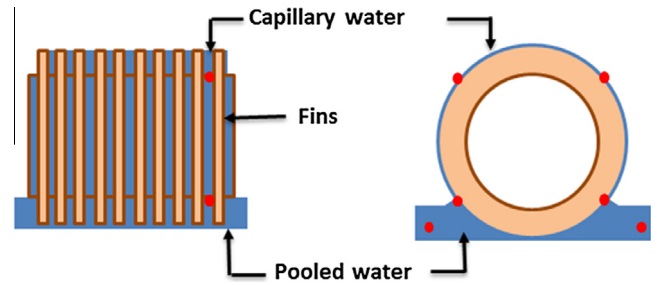


Fig. 2. Schematic of capillary-assisted evaporation. The red dots indicate the positions of thermocouples. (For interpretation of the references to color in this figure legend, the reader is referred to the web version of this article.)

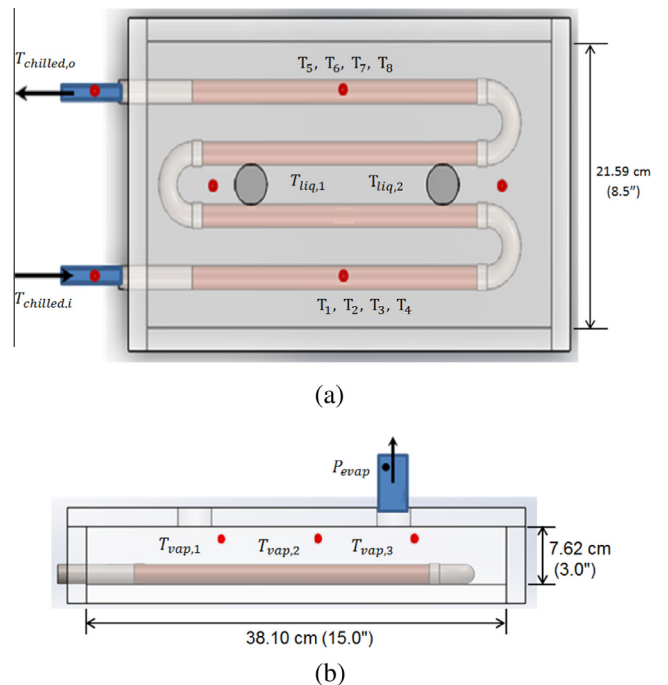


Fig. 3. Capillary-assisted evaporator built for testing different enhanced tubes: (a) top view, and (b) side view. Red dots indicate the location of thermocouples. (For interpretation of the references to color in this figure legend, the reader is referred to the web version of this article.)

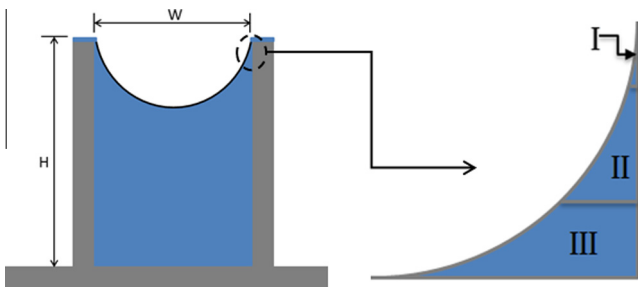


Fig. 1. Evaporating meniscus inside a rectangular-groove.

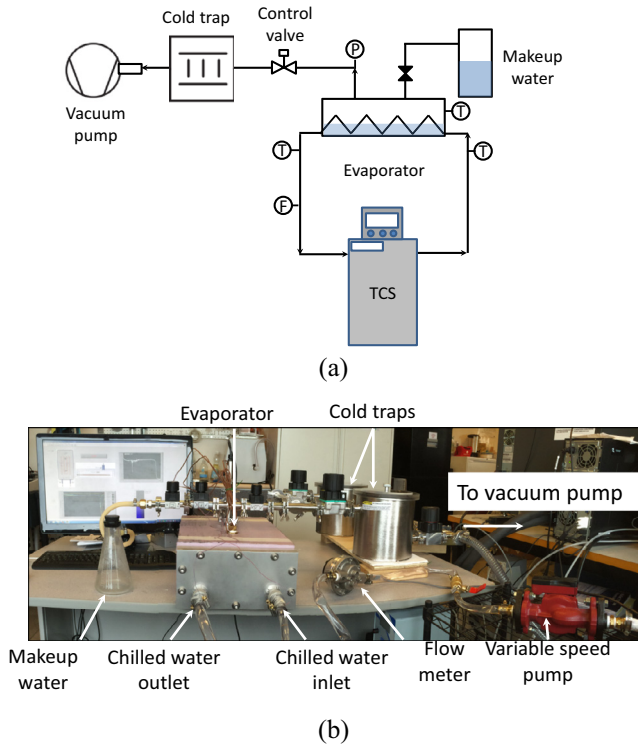


Fig. 4. (a) Schematic of the experimental setup and (b) its photograph.

Table 1
Operating conditions for the experiments.

Parameter	Values		
Chilled water inlet temperatures	10 °C	15 °C	20 °C
Chilled water flow rate	2.3–2.5 kg/min	2.3–2.5 kg/min	2.3–2.5 kg/min
Evaporator pressure	0.8 kPa	1.1 kPa	1.5 kPa
Amount of water in the evaporator at start of experiment	1200 g	1200 g	1200 g

vacuum pump and cold trap were used to mimic an adsorber bed of an ACS. The cold trap, filled with a dry ice and isopropyl alcohol solution, was used to protect the vacuum pump from the water vapor coming from the evaporator. The operating conditions during the experiments are summarized in Table 1. Once the evaporator was evacuated using the vacuum pump, the evaporator was filled with water (1200 g) to immerse the evaporator tube in water. When all the temperatures and pressure inside the evaporator became constant, the control valve was opened and adjusted until the evaporator pressure reached a specific value listed in Table 1. No water was added during the course of the experiment, so the water level dropped until all of the water in the chamber evaporated. The tests were conducted for three types of commercially available enhanced tubes with different fin structures and one plain tube, as a benchmark, as listed in Table 2.

3.1. Data analysis

The operating conditions were kept constant and monitored until a steady-state condition was reached. The chilled water inlet and outlet temperatures, $T_{\text{chilled},i}$ and $T_{\text{chilled},o}$, and the mass flow rate were used to calculate the heat flow rate [32]:

$$\dot{Q}_{\text{evap}}(W) = \dot{m}_{\text{chilled}} c_{p,\text{chilled}} (T_{\text{chilled},i} - T_{\text{chilled},o}) \quad (1)$$

The total evaporation rate, \dot{Q}_{evap} , is calculated by time averaging the heat flow rate given in Eq. (1):

$$\dot{Q}_{\text{evap}}(W) = \frac{\int_{t_1}^{t_2} \dot{q}_{\text{evap}} dt}{t_2 - t_1} \quad (2)$$

where t_1 and t_2 are the beginning and end of the time when the temperatures in the evaporator remain constant. Finally, the overall evaporator heat transfer conductance, UA , is given by:

$$UA = \frac{\dot{Q}_{\text{evap}}}{\Delta T_{\text{LM, evap}}} \quad (3)$$

where A is the nominal surface area of the tubes and $\Delta T_{\text{LM, evap}}$ is the logarithmic mean temperature difference between the chilled water and the refrigerant:

$$\Delta T_{\text{LM, evap}} = \frac{T_{\text{chilled},i} - T_{\text{chilled},o}}{\ln \left(\frac{T_{\text{chilled},i} - T_{\text{liq}}}{T_{\text{chilled},o} - T_{\text{liq}}} \right)} \quad (4)$$

where T_{liq} is the average of $T_{\text{liq},1}$ and $T_{\text{liq},2}$, as shown in Fig. 3a. Eq. (5) gives the external heat transfer coefficient (h_o):

$$h_o = \frac{\dot{Q}_{\text{evap}}}{A_o(\Delta T)} \quad (5)$$

where ΔT is the difference between tube wall temperature, T_{wall} , and liquid refrigerant temperature, T_{liq} :

$$T_{\text{wall}} = \frac{1}{8} \sum_{i=1}^8 T_i \quad (6)$$

$$T_{\text{liq}} = \frac{1}{2} (T_{\text{liq},1} + T_{\text{liq},2}) \quad (7)$$

Finally, the internal heat transfer coefficient (h_i) of enhanced tubes is deduced using Eq. (8) [33]:

$$\frac{1}{UA} = \left(\frac{1}{h_o A_o} + \frac{1}{h_i A_i} + R_{o,\text{finned tube}} \right) \quad (8)$$

The first term on the right hand side of Eq. (8) describes the external convective heat resistance due to evaporation on the external surface of the tube, the second term is the internal convective heat resistance due to single-phase flow inside the tube, and the third term is the conductive heat resistance of the tube wall. From the analysis shown in Appendix A, the internal convective heat resistance is calculated. The internal heat transfer coefficient (h_i) of the plain tube is calculated using the following relation

$$\frac{1}{UA} = \frac{1}{h_o A_o} + \frac{1}{h_i A_i} + \frac{\ln(r_o/r_i)}{2\pi kL} \quad (9)$$

The effectiveness (ε) and number of transfer units (NTU) of the LP evaporator are calculated by Eqs. (10) and (11), respectively.

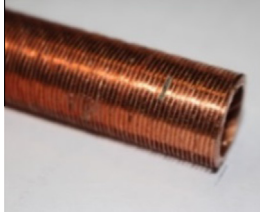



$$\varepsilon = \frac{\dot{Q}_{\text{evap}}}{\dot{Q}_{\text{max}}} = \frac{\dot{m}_{\text{chilled}} c_{p,\text{chilled}} (T_{\text{chilled},i} - T_{\text{chilled},o})}{\dot{m}_{\text{chilled}} c_{p,\text{chilled}} (T_{\text{chilled},i} - T_{\text{liq}})} = \frac{T_{\text{chilled},i} - T_{\text{chilled},o}}{T_{\text{chilled},i} - T_{\text{liq}}} \quad (10)$$

$$NTU = \frac{UA}{\dot{m}_{\text{chilled}} c_{p,\text{chilled}}} \quad (11)$$

4. Uncertainty analysis

The systematic uncertainty [34] in calculation of U was 1.1% and the random uncertainty in the measurement of U over time was 7%. Thus, the maximum uncertainty in the calculation of U was 8%. The systematic uncertainty in calculation of h_o was equal to 1.5% and the random uncertainty in the measurement of h_o over

Table 2
Technical specifications of the enhanced tubes used for the experiments.

Tube name and details	Fin structure	5× zoom view
Turbo Chil-26 FPI (Wolverine Tube Inc.) OD: 19.05 mm (3/4") Fin height: 1.422 mm Min. wall under fins: 0.737 mm Inside surface area: 0.049 m ² /m Outside surface area: 0.193 m ² /m		
Turbo Chil-40 FPI (Wolverine Tube Inc.) OD: 19.05 mm (3/4") Fin height: 1.473 mm Min. wall under fins: 0.635 mm Inside surface area: 0.051 m ² /m Outside surface area: 0.263 m ² /m		
GEWA-KS-40 FPI (Wieland Thermal Solutions) OD: 19.05 mm (3/4") Fin height: 0.9 mm Min. wall under fins: 0.7 mm Inside surface area: 0.0489 m ² /m Outside surface area: 0.194 m ² /m		
Plain tube OD: 19.05 mm (3/4") Inside surface area: 0.0547 m ² /m Outside surface area: 0.0598 m ² /m		

time was 9.0%. Therefore, the maximum uncertainty in the calculation of h_o was 10.5%. The detailed calculations of the total uncertainties for U and h_o are shown in Appendix B.

5. Results and discussion

The operating pressure and temperature of the evaporator versus time for a GEWA-KS-40 FPI, provided by Wieland Thermal Solution, IL, USA, tube at a constant chilled water inlet temperature of 15 °C are shown in Fig. 5. It can be seen in Fig. 5a that the initial evaporator pressure is higher than the saturation pressure of water at 15 °C due to dissolved gases from the makeup water. The evaporator pressure decreases once the control valve is opened and remains constant until the evaporator runs out of water, at which time the pressure drops suddenly. Fig. 5b shows that all of the thermocouples have the same reading at the beginning of the test (equilibrium state). After opening the control valve, the evaporation temperature is set by the evaporation pressure. The locations of the thermocouples measuring the wall temperatures are shown in Fig. 3a.

Fig. 6 shows the effect of capillary phenomenon on the performance of an evaporator built with a GEWA-KS-40 FPI tube at chilled water inlet temperature of 15 °C compared with the one built with plain tubes. As shown in Fig. 6a, the GEWA-KS-40 FPI tube results in an increasing h_o over time. Even as the height of the liquid decreases, the capillary action ensures that the entire outside surface of the tube remains covered and the external heat transfer is characterized by the thin film evaporation. As seen in Fig. 2, the external surface of the tube is covered by pooled water

and capillary water. As the height of the liquid falls, the hydrostatic pressure in the pooled water column decreases. This drop in hydrostatic pressure allows the saturation temperature of the liquid column to drop as well. Fig. 6a also suggests that the effect of liquid level is an important parameter to achieve higher external heat transfer coefficient from capillary-assisted evaporators. Fig. 6b shows that the plain tube fails to maintain the external heat transfer rate and, consequently, h_o drops as the height of the liquid water inside the evaporator drops. As the level of the liquid water drops and since there is no capillary action, the evaporation is mainly due to pool boiling. Even if there is a decrease in hydrostatic pressure as the level drops, the heat transfer surface area available for the pool boiling is also decreased.

The variation of external heat transfer coefficient (h_o) and overall heat transfer coefficient (U) against the chilled water temperature are shown in Fig. 7. As shown in Fig. 7a, increasing the chilled water inlet temperature results in higher evaporation temperature. A higher evaporation temperature increases the thermal conductivity and decreases the viscosity of the liquid film around the tube, thereby increasing h_o . The results shown in Fig. 7a indicate positive correlation between h_o and chilled water inlet temperature. When the chilled water inlet temperature is increased from 10 to 20 °C, h_o varies from 2800 to 5030 W/m² K for Turbo Chil-40 FPI tube. As shown in Fig. 7a, the enhanced tubes result in an average h_o increase of 3.9, 4.2, and 3.9 times compared to the plain tube at chilled water inlet temperatures of 10, 15, and 20 °C, respectively. The Turbo Chil-40 FPI tube provides the highest h_o of 5030 W/m² K at the chilled water inlet temperature of 20 °C, followed by Turbo Chil-26 FPI. The variations of overall heat transfer coefficient, U ,

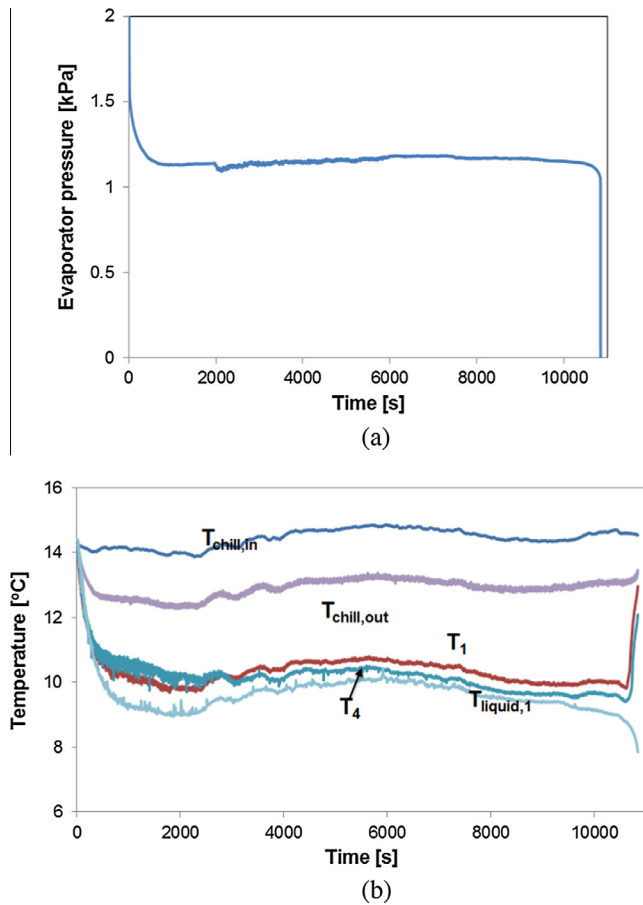


Fig. 5. The behavior of evaporator with GEWA-KS-40 FPI at the chilled water inlet temperature of 15 °C vs. time: (a) evaporator pressure and (b) temperature at different locations in the evaporator.

against the chilled water temperature are presented in Fig. 7b. The U also has positive correlation with chilled water inlet temperature. The chilled water inlet temperature has positive influence on both h_i and h_o , and therefore, increases the overall heat transfer coefficient (U) of the enhanced tubes. Fig. 7b depicts the overall heat transfer coefficient, U , as high as 1098 W/(m² K) can be achieved by using Turbo Chil-40 FPI at chilled water inlet temperatures of 20 °C. While, the plain tube has an U of only 533 W/(m² K), which is 51% lower than the Turbo Chil-40 FPI.

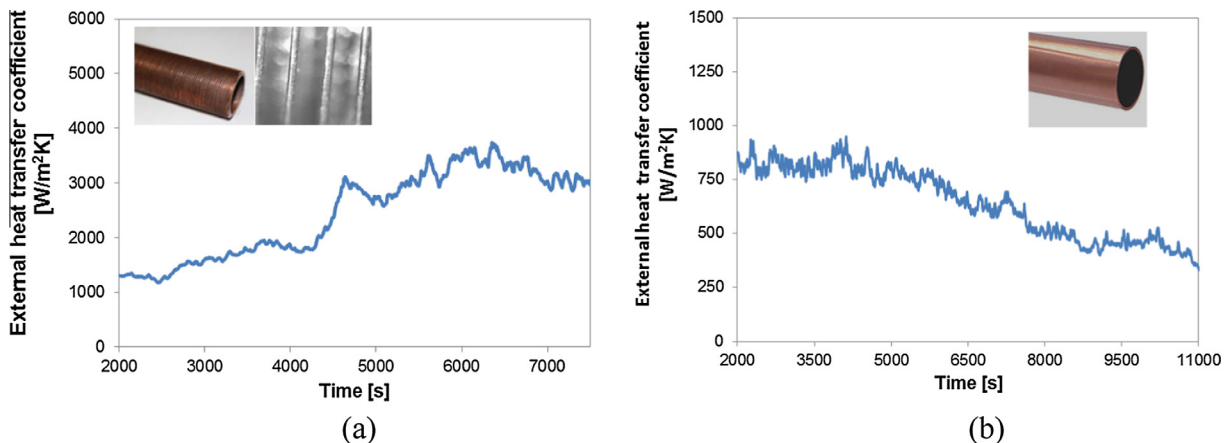


Fig. 6. External heat transfer coefficient achieved by using (a) Wieland's GEWA-KS-40 FPI tube, and (b) plain tube.

Comparing the h_o provided by the enhanced tubes shown in Fig. 7a and fin structures shown in Table 2 indicates that the two most important parameters in the design of capillary-assisted evaporators are to have continuous parallel fins, such as Turbo Chil-40 FPI and Turbo Chil-26 FPI, and high heat transfer surface area. Comparing the results of the Turbo Chil-26 FPI and GEWA-KS-40 FPI which have the same heat transfer surface area (both internal and external), and similar continuous parallel fins indicates that Turbo Chil-26 FPI with lower fin density provides higher h_o compared to GEWA-KS-40 FPI with higher fin density. This is because Turbo Chil-26 FPI has a higher fin height by 58% which contributes more effectively in the capillary evaporation.

To generate cooling in an evaporator, the heat has to be transferred from the chilled liquid water flowing inside the tube, to the tube wall, and finally, to the refrigerant. Therefore, the thermal resistances to the heat flow when heat is transferred from the chilled water to the refrigerant should be evaluated. Fig. 8 shows the comparison of different thermal resistances in a Turbo Chil-40 FPI tube. Due to high h_o achieved from capillary-assisted evaporation combined with higher outer surface area (A_o), the external convection resistance, $1/(h_o A_o)$, of the enhanced tube is smaller than the internal convection resistance, $1/(h_i A_i)$. The single-phase heat transfer in the chilled waterside results in lower h_i . As shown in Fig. 8, the internal thermal resistances are 14.8, 16.8, and 18.1 times higher than the external thermal resistances at the chilled water inlet temperatures of 10, 15, and 20 °C, respectively. Using Eq. (8), the overall resistance is evaluated. When the chilled water temperature is increased from 10 to 20 °C, the overall resistance drops from 0.014 to 0.0098 K/W for Turbo Chil-40 FPI tube. One can notice from Fig. 8 that the internal convection resistance ($1/h_i A_i$) controls the overall heat transfer resistance ($1/UA$).

The comparison of thermal resistances for different tubes at chilled water inlet temperature of 20 °C is shown in Fig. 9. It can be seen in Fig. 9 that the conductive resistance of the fin tubes is higher than the plain tube. The conductive resistances of enhanced tubes depend upon the overall fin efficiency ($\eta_{o,fin}$) and h_o . In Eq. (8), h_o appears in both external convective heat resistance and conductive resistance terms. Therefore, increasing h_o of the enhanced tubes can be favorable to reduce the overall resistance of the evaporator. For the plain tube, both internal and external convective resistances contribute to the overall heat transfer resistance almost equally. For the enhanced tubes, the external convective resistance is much smaller than the internal convective resistance due to enhancement on the outside surface of the tube and the capillary evaporation. For the enhanced tubes, an average of 85% of the overall thermal resistance is due to the internal convective resistance,

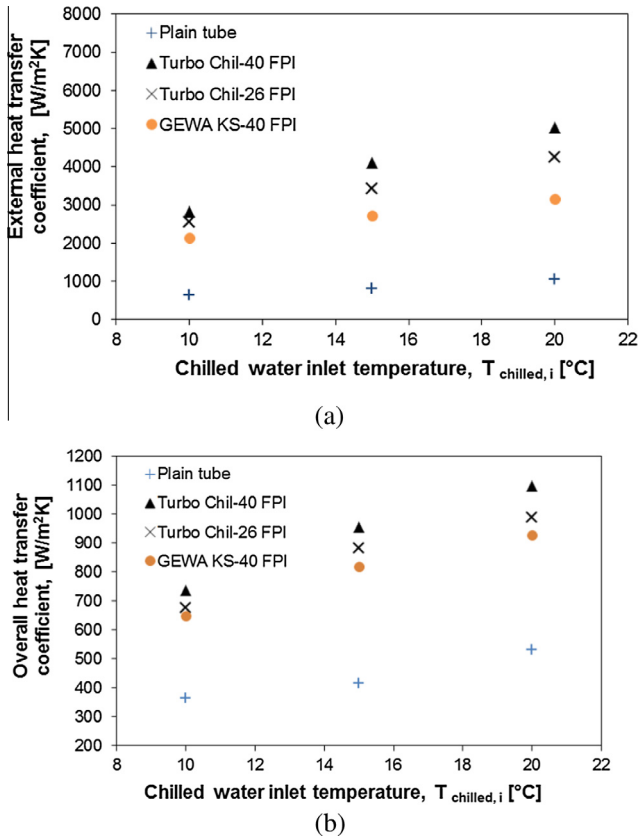


Fig. 7. (a) The external heat transfer coefficient, and (b) the overall heat transfer coefficient for three different enhanced tubes and one plain tube.

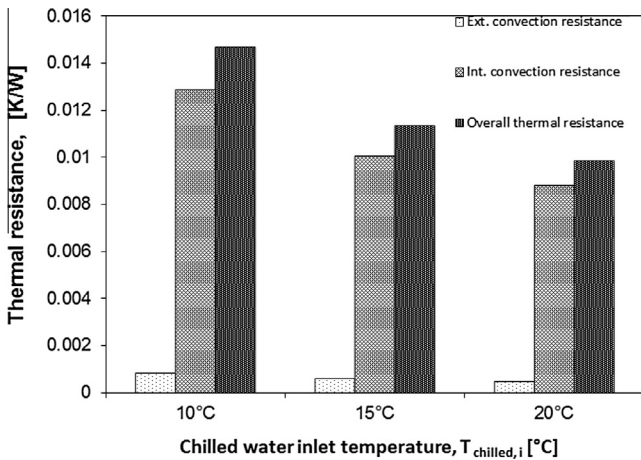


Fig. 8. Comparison of thermal resistances for the LP evaporator built with a Turbo Chil-40 FPI tube.

while the conductive and external convective resistances contribute to only 8% and 7% of the overall thermal resistance, respectively. Therefore, one can conclude that the internal heat transfer resistance controls the overall heat transfer resistance and is the main hindrance to the heat transfer. The overall thermal resistance in Fig. 9 suggests that in order to improve the thermal performance of a LP evaporator, the internal convective resistance should reduce by increasing both h_i and A_i .

The ϵ -NTU shown in Fig. 10 can be of great practical utility in designing a LP evaporator. The effectiveness (ϵ) and NTU are calculated using Eqs. (10) and (11), respectively. Turbo Chil-40 FPI yields

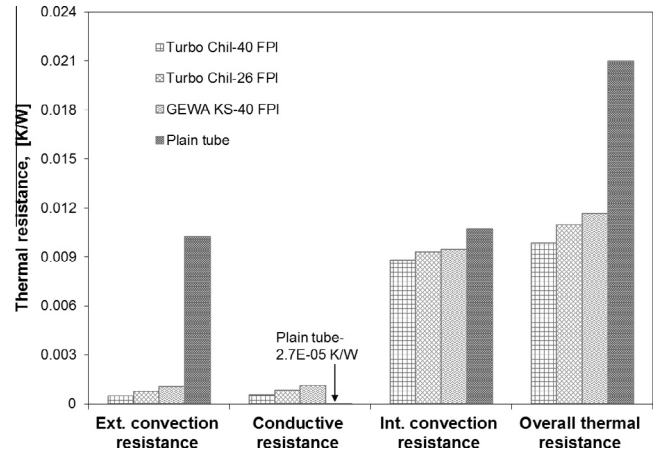


Fig. 9. Comparison of thermal resistances for three different enhanced tubes and one plain tube at chilled water inlet temperature of 20 °C.

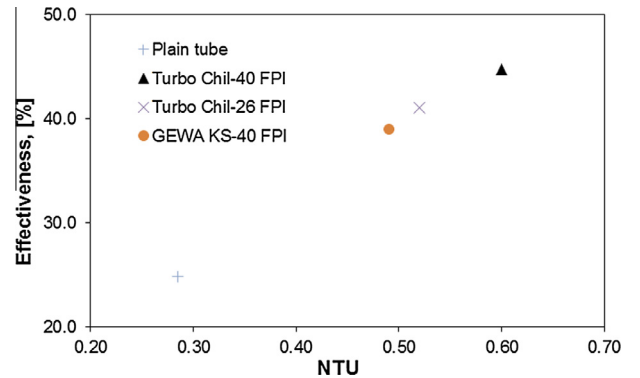


Fig. 10. Effectiveness, ϵ , of the LP evaporator with capillary-assisted tubes vs. NTU.

the highest ϵ and NTU of 45% and 0.6 at the chilled water inlet temperature of 20 °C, respectively. Evaporator's built using enhanced tubes provided 1.8 times higher effectiveness than that built with plain tubes. However, the effectiveness of the present design is still limited due to the poor internal heat transfer. To increase ϵ , the internal convective heat transfer resistance should be decreased. In addition, for higher ϵ , one must increase the UA value by increasing the overall heat transfer coefficient and the length of the tube. Increasing the length of the tubes increases the size (and cost) of the LP evaporator. Therefore, for a constant tube length and diameter, one should employ heat transfer augmentation techniques at the inside of the tube to decrease the internal convective resistance ($1/h_i A_i$), and consequently, increase the effectiveness.

6. Conclusion

In this paper, a LP evaporator with capillary-assisted tubes was proposed for ACS with vehicle A/C applications. The evaporator consisted of horizontal capillary-assisted tubes in contact with a pool of water. The evaporator pressure was maintained between 0.8 and 1.5 kPa. In this study, three different tubes with various fin geometries were experimentally investigated and their effects on the external and overall heat transfer coefficients were examined. The performances of the capillary-assisted tubes were compared with that of plain tube. The capillary action on the surface of the enhanced tubes provided an increase in external heat transfer coefficient when the height of the liquid water in

the evaporator was decreased. The enhanced tubes indicated a positive correlation between the external heat transfer coefficient (h_o) and the chilled water inlet temperature. The experimental results indicated that the Turbo Chil-40 FPI with higher fin density and fin height provided the highest external heat transfer coefficient of 5030 W/m² K, when compared to Turbo Chil-26 FPI and GEWA-KS-40 FPI tubes. The Turbo Chil-40 FPI provided the lowest overall heat transfer resistance among the tested commercially available enhanced tubes. For the enhanced tubes, up to 89% of the overall thermal resistance was due to the internal convective resistance. For the plain tube, 48.8% and 51% of the overall thermal resistance was due to the external and internal convective resistances, respectively. The maximum effectiveness and NTU achieved were 45% and 0.6, respectively, for the Turbo Chil-40 FPI at chilled water inlet temperature of 20 °C. The main bottleneck in the performance of a LP evaporator was the internal heat transfer.

Acknowledgement

The authors gratefully acknowledge the financial support of the Natural Sciences and Engineering Research Council of Canada (NSERC) through Automotive Partnership Canada Grant No. APCPJ 401826-10. The authors are thankful to Wolverine Tube Inc. and Wieland Thermal Solutions for assisting our research by providing enhanced tubes.

Appendix A

To calculate the internal convective resistance due to a fluid circulated in a finned tube, the following steps should be taken. The tubes of interest in this study have circumferential, rectangular cross-section fins. The efficiency of a fin located on the surface of the tube with circumferential, rectangular cross-section fins can be calculated from Eqs. (A1)–(A5) [33]:

$$\eta_f = C \frac{(K_1(mr_1)I_1(mr_{2c}) - I_1(mr_1)K_1(mr_{2c}))}{I_0(mr_1)K_1(mr_{2c}) + K_0(mr_1)I_1(mr_{2c})} \quad (A1)$$

$$C = \frac{(2r_1/m)}{(r_{2c}^2 - r_1^2)} \quad (A2)$$

$$m = \sqrt{\frac{2h}{kt_f}} \quad (A3)$$

$$r_{2c} = r_2 + (t_f/2) \quad (A4)$$

$$A_f = 2\pi(r_{2c}^2 - r_1^2) \quad (A5)$$

where r_1 and r_2 are the distances from the center of the tube to the fin base and fin tip, respectively. I_0 , and K_0 in Eq. (A1) are modified, zero-order Bessel functions of the first and second kinds, respectively. I_1 , and K_1 in Eq. (A1) are modified, first-order Bessel functions of the first and second kinds, respectively. t_f in Eq. (A3) is the fin thickness and A_f in Eq. (A5) is the fin heat transfer surface area. The total external heat transfer surface area of the finned tube is calculated as follows:

$$A_t = N(A_f + A_b) \quad (A6)$$

$$A_b = 2\pi r_1 t_b \quad (A7)$$

where N is the total number of fins, and A_b and t_b are the prime (plain) heat transfer surface area of the finned tube and the space between two fins, respectively. Using Eqs. (A1), (A5), and (A6), the overall efficiency of the finned tube can be calculated [33]:

$$\eta_{o,fin} = 1 - \frac{A_f}{A_f + A_b}(1 - \eta_f) \quad (A8)$$

Consequently, the conductive heat transfer resistance due to the fins of the finned tube can be estimated.

$$R_{fin} = \frac{1}{\eta_{o,fin} h_o A_t} \quad (A9)$$

where the convection coefficient h_o is measured in the experiment. Also, the conductive resistance of wall located under the fins can be calculated as follows:

$$R_{wall} = \frac{\ln(r_1/r_0)}{2\pi kL} \quad (A10)$$

where r_0 and L are the internal radius and length of the finned tube, respectively. R_{fin} and R_{wall} are thermal resistances in series. Therefore, the overall conductive resistance of the finned tube is calculated by Eq. (A11).

$$R_{o,finned\ tube} = R_{fin} + R_{wall} \quad (A11)$$

Finally, Eq. (A12) gives the internal convective heat transfer resistance of the finned tube.

$$\frac{1}{h_i A_i} = \frac{1}{UA} - \left(\frac{1}{h_o A_o} + R_{o,finned\ tube} \right) \quad (A12)$$

From the experimental data measurements, the capillary evaporation coefficient on the external surface of a finned tube can be calculated. Information required to calculate the internal convective resistance of enhanced tubes at 20 °C chilled water inlet temperature are listed in Table A1.

By substituting the values given in Table A1, the thermal resistances of tubes can be determined as shown in Table A2.

Table A1
Details to calculate internal convective resistance of enhanced tubes.

Parameter	Turbo Chil-40 FPI	Turbo Chil-26 FPI	GEWA-KS-40 FPI	Plain tube
L	1.54 m	1.54 m	1.54 m	1.54 m
r_0	7.417×10^{-3} m	7.417×10^{-3} m	7.417×10^{-3} m	8.712×10^{-3} m
r_1	8.052×10^{-3} m	8.103×10^{-3} m	8.625×10^{-3} m	9.525×10^{-3} m
r_2	9.525×10^{-3} m	9.525×10^{-3} m	9.525×10^{-3} m	–
t_f	1.59×10^{-4} m	2.24×10^{-4} m	1.30×10^{-4} m	–
t_b	4.76×10^{-4} m	7.53×10^{-4} m	5.05×10^{-4} m	–
h_o	5030 W/m ² K	4254 W/m ² K	3152 W/m ² K	1045 W/m ² K
k	340 W/m K	340 W/m K	340 W/m K	340 W/m K
A_t	0.41 m ²	0.30 m ²	0.30 m ²	0.0922 m ²
A	0.0922 m ²	0.0922 m ²	0.0922 m ²	0.0893 m ²
A_i	0.0796 m ²	0.0764 m ²	0.0764 m ²	0.08537 m ²

Table A2
Thermal resistances for different tubes.

Parameter	Ext. convection resistance [K/W]	Conductive resistance [K/W]	Int. convection resistance [K/W]	Overall thermal resistance [K/W]
Turbo Chil-40 FPI	4.85×10^{-4}	5.75×10^{-4}	8.81×10^{-3}	9.87×10^{-3}
Turbo Chil-26 FPI	7.81×10^{-4}	8.66×10^{-4}	9.31×10^{-3}	1.09×10^{-2}
GEWA KS-40 FPI	1.04×10^{-3}	1.13×10^{-3}	9.48×10^{-3}	1.16×10^{-2}
Plain tube	1.02×10^{-2}	2.67×10^{-5}	1.07×10^{-2}	2.09×10^{-2}

Appendix B

The systematic uncertainty [34] in the evaporator heat transfer rate calculation is:

$$\left(\frac{\delta \dot{q}_{evap}}{\dot{q}_{evap}}\right)_{systematic} = \sqrt{\left(\frac{\delta \dot{m}_{chilled}}{\dot{m}_{chilled}}\right)^2 + \left(\frac{\delta(T_{chilled,i} - T_{chilled,o})}{T_{chilled,i} - T_{chilled,o}}\right)^2} \quad (B1)$$

where,

$$\frac{\delta(T_{chilled,i} - T_{chilled,o})}{T_{chilled,i} - T_{chilled,o}} = \sqrt{\left(\frac{\delta T_{chilled,i}}{T_{chilled,i}}\right)^2 + \left(\frac{\delta T_{chilled,o}}{T_{chilled,o}}\right)^2} = \sqrt{0.0075^2 + 0.0075^2} = 0.01 \quad (B2)$$

Thus, the maximum systematic uncertainty in the calculation of evaporator heat transfer rate is:

$$\left(\frac{\delta \dot{q}_{evap}}{\dot{q}_{evap}}\right)_{systematic} \times 100 = \sqrt{0.005^2 + 0.01^2} = 1.1\% \quad (B3)$$

Also, the standard deviation for \dot{q}_{evap} due to the random uncertainty is 4.8%. Thus the maximum uncertainty of \dot{q}_{evap} during the experiments is 5.9% (= 1.1% + 4.8%). Eq. (B4) gives the systematic uncertainty of the overall heat transfer coefficient:

$$\left(\frac{\delta U}{U}\right)_{systematic} = \sqrt{\left(\frac{\delta \dot{Q}_{evap}}{\dot{Q}_{evap}}\right)_{systematic}^2 + \left(\frac{\delta \Delta T_{LM, evap}}{\Delta T_{LM, evap}}\right)^2} \quad (B4)$$

where $\left(\frac{\delta \dot{Q}_{evap}}{\dot{Q}_{evap}}\right)_{systematic}$ and $\frac{\delta \Delta T_{LM, evap}}{\Delta T_{LM, evap}}$ are equal to 1.1% and 0.04%, respectively. Therefore, $\left(\frac{\delta U}{U}\right)_{systematic}$ is equal to 1.1% (\approx (1.1% + 0.04%). The random uncertainty in the measurement for U_{evap} over time is 6.8%. Thus, the maximum uncertainty in the calculation of overall heat transfer coefficient is 7.9% (= 1.1% + 6.8%). Eq. (B5) gives the systematic uncertainty of the external heat transfer coefficient:

$$\left(\frac{\delta h_o}{h_o}\right)_{systematic} = \sqrt{\left(\frac{\delta \dot{Q}_{evap}}{\dot{Q}_{evap}}\right)_{systematic}^2 + \left(\frac{\delta \Delta T}{\Delta T}\right)^2} \quad (B5)$$

where $\left(\frac{\delta \dot{Q}_{evap}}{\dot{Q}_{evap}}\right)_{systematic}$ and $\frac{\delta \Delta T}{\Delta T}$ are equal to 1.1% and 1% (similar to Eq. (B2)), respectively. Therefore, $\left(\frac{\delta h_o}{h_o}\right)_{systematic}$ is equal to 1.5%. The random uncertainty in the measurement for h_o over time is 9.0%. Thus, the maximum uncertainty in the calculation of external heat transfer coefficient is 10.5% (= 1.5% + 9.0%).

References

[1] William Goetzler, Robert Zogg, C.J. Johnson, Jim Young, Energy savings potential and RD & D opportunities for non-vapor-compression HVAC, Energy Effic Renew Energy (2014) 3673.
 [2] B.Y.W. Goetzler, M. Ashrae, R. Zogg, M. Ashrae, J.I.M. Young, A.M. Ashrae, et al., Alternatives to HVAC technology, ASHRAE J (2014) 12–23.
 [3] Martin F. Weilenmann, Robert Alvarez, M. Keller, Fuel consumption and CO₂/pollutant emissions of mobile air conditioning at fleet level - new data and model comparison, Environ. Sci. Technol. 44 (2010) 5277–5282.

[4] M. Suzuki, Application of adsorption cooling systems to automobiles, Heat Recov Syst CHP 13 (1993) 335–340.
 [5] R. Farrington, J. Rugh, Impact of vehicle air-conditioning on fuel economy, tailpipe emissions, and electric vehicle range, Fuel (2000). <http://www.nrel.gov/docs/fy00osti/28960.pdf>. doi: NREL/CP-540-28960.
 [6] M.O. Abdullah, I.A.W. Tan, L.S. Lim, Automobile adsorption air-conditioning system using oil palm biomass-based activated carbon: a review, Renew. Sustain. Energy Rev. 15 (2011) 2061–2072, <http://dx.doi.org/10.1016/j.rser.2011.01.012>.
 [7] L. Schnabel, K. Witte, J. Kowol, P. Schossig, Evaluation of different evaporator concepts for thermally driven sorption heat pumps and chiller, Int. Sorption Heat Pump Conf., Padua, Italy (2011) 525–543.
 [8] M.Z.I. Khan, K.C.A. Alam, B.B. Saha, A. Akisawa, T. Kashiwagi, Study on a re-heat two-stage adsorption chiller – the influence of thermal capacitance ratio, overall thermal conductance ratio and adsorbent mass on system performance, Appl. Therm. Eng. 27 (2007) 1677–1685, <http://dx.doi.org/10.1016/j.applthermaleng.2006.07.005>.
 [9] Y.L. Liu, R.Z. Wang, Z.Z. Xia, Experimental performance of a silica gel-water adsorption chiller, Appl. Therm. Eng. 25 (2005) 359–375, <http://dx.doi.org/10.1016/j.applthermaleng.2004.06.012>.
 [10] F. Lanzerath, U. Bau, J. Seiler, A. Bardow, Optimal design of adsorption chillers based on a validated dynamic object-oriented model, Sci. Technol. Built. Environ. 21 (2015) 248–257, <http://dx.doi.org/10.1080/10789669.2014.990337>.
 [11] L. Schnabel, C. Scherr, C. Weber, Water as refrigerant – experimental evaluation of boiling characteristics at low temperatures and pressures, VII Minsk Int Semin “Heat Pipes, Heat Pumps, Refrig Power Sources” (2008) 322–330.
 [12] J. Castro, J. Farns, A. Oliva, E. Garca-Rivera, Flooded evaporators for LiBr–H₂O absorption chillers: modelling and validation, Proc. 8th IIR Gustav Lorentzen Nat. Work. Fluids Conf. (2008) 217–223.
 [13] G.A. Florides, S.A. Kalogirou, S.A. Tassou, L.C. Wrobel, Design and construction of a LiBr–water absorption machine, Energy Convers. Manage. 44 (2003) 2483–2508, [http://dx.doi.org/10.1016/S0196-8904\(03\)00006-2](http://dx.doi.org/10.1016/S0196-8904(03)00006-2).
 [14] J. Castro, A. Oliva, C.D. Perez-Segarra, C. Oliet, Modelling of the heat exchangers of a small capacity, hot water driven, air-cooled H₂O–LiBr absorption cooling machine, Int. J. Refrig 31 (2008) 75–86, <http://dx.doi.org/10.1016/j.ijrefrig.2007.05.019>.
 [15] G. Ribatski, A.M. Jacobi, Falling-film evaporation on horizontal tubes – a critical review, Int. J. Refrig 28 (2005) 635–653, <http://dx.doi.org/10.1016/j.ijrefrig.2004.12.002>.
 [16] L. Yang, S. Shen, Experimental study of falling film evaporation heat transfer outside horizontal tubes, Desalination 220 (2008) 654–660, <http://dx.doi.org/10.1016/j.desal.2007.02.046>.
 [17] W. Li, X.Y. Wu, Z. Luo, S.C. Yao, J.L. Xu, Heat transfer characteristics of falling film evaporation on horizontal tube arrays, Int. J. Heat Mass Transf. 54 (2011) 1986–1993, <http://dx.doi.org/10.1016/j.ijheatmasstransfer.2010.12.031>.
 [18] W. Li, X.Y. Wu, Z. Luo, R.L. Webb, Falling water film evaporation on newly-designed enhanced tube bundles, Int. J. Heat Mass Transf. 54 (2011) 2990–2997, <http://dx.doi.org/10.1016/j.ijheatmasstransfer.2011.02.052>.
 [19] H.M. Sabir, Y.B.M. Elhag, Experimental study of capillary-assisted evaporators, Energy Build. 40 (2008) 399–407, <http://dx.doi.org/10.1016/j.enbuild.2007.02.036>.
 [20] H.M. Sabir, A.C. Bwalya, Experimental study of capillary-assisted water evaporators for vapour-absorption systems, Appl. Energy 71 (2002) 45–57, [http://dx.doi.org/10.1016/S0306-2619\(01\)00042-3](http://dx.doi.org/10.1016/S0306-2619(01)00042-3).
 [21] H.M. Sabir, Y.B.M. ElHag, A study of capillary-assisted evaporators, Appl. Therm. Eng. 27 (2007) 1555–1564, <http://dx.doi.org/10.1016/j.applthermaleng.2006.09.011>.
 [22] Z.Z. Xia, G.Z. Yang, R.Z. Wang, Capillary-assisted flow and evaporation inside circumferential rectangular micro groove, Int. J. Heat Mass Transf. 52 (2009) 952–961, <http://dx.doi.org/10.1016/j.ijheatmasstransfer.2008.05.041>.
 [23] Z.Z. Xia, G.Z. Yang, R.Z. Wang, Experimental investigation of capillary-assisted evaporation on the outside surface of horizontal tubes, Int. J. Heat Mass Transf. 51 (2008) 4047–4054, <http://dx.doi.org/10.1016/j.ijheatmasstransfer.2007.11.042>.
 [24] D.C. Wang, Z.Z. Xia, J.Y. Wu, R.Z. Wang, H. Zhai, W.D. Dou, Study of a novel silica gel–water adsorption chiller. Part I. Design and performance prediction, Int. J. Refrig 28 (2005) 1073–1083, <http://dx.doi.org/10.1016/j.ijrefrig.2005.03.001>.
 [25] F. Lanzerath, J. Seiler, M. Erdogan, H. Schreiber, M. Steinhilber, A. Bardow, The impact of filling level resolved: capillary-assisted evaporation of water for

- adsorption heat pumps, *Appl. Therm. Eng.* 102 (2016) 513–519, <http://dx.doi.org/10.1016/j.applthermaleng.2016.03.052>.
- [26] F. Lanzerath, M. Erdogan, H. Schreiber, M. Steinhilber, A. Bardow, Combination of finned tubes and thermal coating for high performance water evaporation in adsorption heat pumps, *Int. Sorption Heat Pump Conf.* (2014) 1–10.
- [27] R.H. Nilson, S.W. Tchikanda, S.K. Griffiths, M.J. Martinez, Steady evaporating flow in rectangular microchannels, *Int. J. Heat Mass Transf.* 49 (2006) 1603–1618, <http://dx.doi.org/10.1016/j.ijheatmasstransfer.2005.11.002>.
- [28] H.B. Ma, G.P. Peterson, Temperature variation and heat transfer in triangular grooves with an evaporating film, *J. Thermophys. Heat Transf.* 11 (1997) 90–97, <http://dx.doi.org/10.2514/2.6205>.
- [29] Z.-H. Kou, H.-T. Lv, W. Zeng, M.-L. Bai, J.-Z. Lv, Comparison of different analytical models for heat and mass transfer characteristics of an evaporating meniscus in a micro-channel, *Int. Commun. Heat Mass Transf.* 63 (2015) 49–53, <http://dx.doi.org/10.1016/j.icheatmasstransfer.2015.02.005>.
- [30] P. Cheng, J. Dong, S.M. Thompson, H.B. Ma, Heat transfer in the bulk and thin film fluid regions of a rectangular micro groove, *J. Thermophys. Heat Transf.* 26 (2012) 108–114, <http://dx.doi.org/10.2514/1.T3684>.
- [31] H.B. Ma, P. Cheng, B. Borgmeyer, Y.X. Wang, Fluid flow and heat transfer in the evaporating thin film region, *Microfluid. Nanofluidics* 4 (2008) 237–243, <http://dx.doi.org/10.1007/s10404-007-0172-5>.
- [32] J.P. Holman, *Heat exchangers*, *Heat Transf.* (2010) 521–587. 10th ed.
- [33] T.L. Bergman, A.S. Lavine, F.P. Incropera, D.P. DeWitt, *Introduction to Heat Transfer*, sixth ed., John Wiley & Sons, 2011.
- [34] J.P. Holman, *Experimental Methods for Engineers*, eighth ed., McGraw-Hill Series in Mechanical Engineering, 2012.